Exciton states and their entanglement in coupled quantum dots

Jia-Lin Zhu,[1,*] Weidong Chu,[1,2] Zhensheng Dai,[1] and Dong Xu[1]
[1]*Department of Physics and Key Lab of Atomic and Molecular Nanoscience, Tsinghua University, Beijing 100084, China*
[2]*Division of Mathematics and Physics, Chinese People's Public Security University, Beijing 100038, China*
(Received 15 August 2005; revised manuscript received 7 September 2005; published 28 October 2005)

Exciton states and optical spectra in a pair of vertically stacked InGaAs/GaAs quantum dots are studied with a proposed variation-diagonalization technique. The spectra obtained are in good agreement with experiments. The tunnel coupling and the exciton entanglement are also investigated. It is found that at short barrier widths, the entanglement is small due to the coupling between the intradot and interdot orbitals. At large barrier widths, large entanglement appears in coupled identical quantum dots; however, such an entanglement can be easily destroyed by the broken symmetry because of the weak tunneling of the hole.

DOI: 10.1103/PhysRevB.72.165346 PACS number(s): 78.67.Hc, 73.21.La

I. INTRODUCTION

Semiconductor quantum dots (QDs) are regarded as "artificial atoms" due to their characteristic discrete energy spectra and controllable physical properties. Corresponding to the similarity between a quantum dot and an atom, a pair of vertically or laterally coupled quantum dots (CQDs) is called a quantum dot molecule. Many efforts have been made to investigate the optoelectronic properties of coupled quantum dots and some moleculelike behaviors induced by the quantum tunneling have been found in these structures. Besides being valuable for the basic physics, coupled quantum dots are of high interest for the physical implementation of solid-state quantum computation.

It has been proposed that the quantum bits (qubits) can be represented by either electron spin states[1–4] or exciton states[5,6] in QDs, and the CQDs can be used as a quantum logical gate to entangle the qubits. Compared with the quantum computation schemes of trapped atoms (ions),[7] nuclear magnetic resonance,[8] cavity quantum electrodynamics[9] and Josephson junctions,[10] the solid-state qubits have relatively long coherence time[11,12] and are suitable for large integration. Recently, with the development of the "indium flush" grow technique,[13] vertically stacked quantum dots of high quality have been fabricated and large interaction-induced energy splittings of exciton states have been observed in the photoluminescence (PL) spectra.[6,14] It has been demonstrated that the coupling of exciton states in CQDs can be controlled by an external electric field[15,16] and an anticrossing induced by the electric field has been directly observed in the PL spectra.[16]

Though the splittings and coupling of exciton states in CQDs have been observed in the PL spectra, so far the exciton entanglement has not been proved directly. In the theoretical analysis of Bayer *et al.*,[6,17] exciton states with large entanglement have been predicted within a symmetric model. In the atomistic pseudopotential calculations of CQDs with consideration of strain modification and alloy fluctuation,[18,19] the entanglement of exciton states has been found to be very small at both small and large interdot separations. Such small entanglement is caused by the broken symmetry induced by the strain and alloy fluctuation. In fact, the entanglements of qubits in CQDs may be influenced by many factors, such as composition fluctuations, dot size differences, and applied external fields. Studying the effects of these factors is important for us to find stable and controllable entanglement in qubits.

In this paper we study exciton states and their entanglements in vertically coupled quantum dots which resemble the experimental system by Bayer *et al.*[6] Under the framework of the effective mass approximation, we provide a variation-diagonalization method to efficiently calculate the exciton states. The evolutions of exciton spectra with varying barrier width and with an external electric field are given and compared with the experimental results. With the analysis of the orbital occupations, the entanglement of exciton states is clearly shown and well explained. The effects of the symmetry, the barrier width, and the external field on the entanglements are systematically studied.

II. MODEL HAMILTONIAN AND VD METHOD

The Hamiltonian of an exciton in vertically coupled InGaAs/GaAs QDs with an electric field can be written as

$$H=\sum_{i=e,h}\left(\frac{\vec{p}_i^{\,2}}{2m_i^*}+q\vec{F}\cdot\vec{r}_i+U_i\right)-\frac{e^2}{4\pi\epsilon_0\epsilon_r|\vec{r}_e-\vec{r}_h|}, \qquad (1)$$

where the one-band model is used for the hole. $q_h(q_e)=e(-e)$, and $\vec{F}$ is an external electric field along the vertical direction. The confining potential U_i is written as

$$U_{i=e,h}=\begin{cases}0 & \text{in QDs},\\ V_i & \text{in surrounding matrix}.\end{cases} \qquad (2)$$

As shown in Fig. 1(a), W_b is the barrier width, $R_{0,1}$ and W_d are dot radii and height, respectively, and V_e and V_h are the conduction and valence band offsets, respectively. In our calculation, W_d depends on the barrier width as shown in Fig. 1(b) and the reason is given in Sec. III.

To efficiently solve the Hamiltonian H of Eq. (1), we propose a variation-diagonalization (VD) method. In the VD method, a trial zeroth-order Hamilton $H_0(\alpha,\beta,\ldots)$, which includes the effective confining potentials U_i^* and effective Coulomb term U_C^* with variational parameters α, β, and so on, is introduced and H is rewritten as

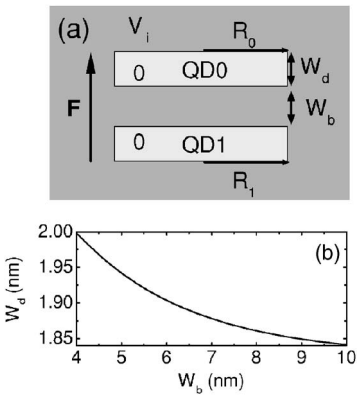

FIG. 1. (a) Schematic illustration of the InGaAs/GaAs coupled quantum dots of radii R_0 and R_1 with height W_d and interdot barrier width W_b; (b) slightly variable W_d as a function of W_b.

$$H = H_0(\alpha, \beta, \ldots) + H'(\alpha, \beta, \ldots). \tag{3}$$

In polar coordinate, H_0 can be written as

$$H_0 = H_{0z} + H_{0\vec{\rho}} \tag{4}$$

with

$$H_{0z} = \sum_{i=e,h} \left(\frac{p_{zi}^2}{2m_i^*} + qFz_i + U_{zi}^* \right) \tag{5}$$

and

$$H_{0\vec{\rho}} = \sum_{i=e,h} \left(\frac{\vec{p}_{\rho i}^2}{2m_i^*} + U_{\rho i}^* \right) + U_C^*. \tag{6}$$

U_{zi}^*, $U_{\rho i}^*$, and U_C^* are as follows:

$$U_{zi}^* = \begin{cases} 0 & \text{for } 0.5W_b \leqslant |z_i| \leqslant W_d + 0.5W_b, \\ V_i & \text{else}, \end{cases} \tag{7}$$

$$U_{\rho i}^* = \alpha_i \rho_i^2, \tag{8}$$

and

$$U_C^* = -\frac{\beta e^2}{4\pi\epsilon_0\epsilon_r |\vec{\rho}_e - \vec{\rho}_h|}, \tag{9}$$

respectively. $H_{0\vec{\rho}}$ can be separated into center-of-mass and relative motion terms:

$$H_{0\vec{\rho}} = H_{0CM} + H_{0rel}, \tag{10}$$

with

$$H_{0CM} = \frac{\vec{p}_{\vec{\rho}CM}^2}{2M} + (\alpha_e + \alpha_h)\rho_{CM}^2 \tag{11}$$

and

$$H_{0rel} = \frac{\vec{p}_{\vec{\rho}rel}^2}{2\mu} + \frac{\alpha_e m_h^{*2} + a_h m_e^{*2}}{M^2}\rho_{rel}^2 - \frac{\beta e^2}{4\pi\epsilon_0\epsilon_r\rho_{rel}}, \tag{12}$$

where $M = m_e^* + m_h^*$ and $\mu = m_e^* m_h^*/(m_e^* + m_h^*)$. The solutions of H_{0CM} can be obtained analytically, and those of H_{0z} and H_{0rel} are exactly obtained by the series expansion method.[20,21] Then a set of variational basis, which can reflect the effects of confining potentials, Coulomb interaction, and external field, is constructed by using the eigenstates of H_0. The variational basis, the eigenstates of the total Hamiltonian H, and the minimal ground state energy are simultaneously determined by both the variation method and the exact diagonalization.

Once the exciton states are obtained, we can calculate directly the measurable properties, such as the linear optical susceptibilities of the CQDs, whose imaginary part is related to optical transition intensity. In theory, the linear optical susceptibility is proportional to the dipole matrix elements between the exciton states Ψ_j and the vacuum state, which in turn are proportional to the oscillator strengths F_j. In the dipole approximation, they are given by[22–24]

$$F_j = \left| \int d\vec{\rho}_{CM} d\vec{\rho}_{rel} dz_e dz_h \Psi_j(\vec{\rho}_{CM}, \vec{\rho}_{rel}, z_e, z_h)\, \delta(\vec{\rho}_{rel}) \times \delta(z_e - z_h) \right|^2. \tag{13}$$

Then the frequency dependence of the linear optical susceptibility $\chi(\omega)$ can be expressed as[22–24]

$$\chi(\omega) \propto \sum_j \frac{F_j}{\hbar\omega - E_g - E_j - i\Gamma}, \tag{14}$$

where E_g and E_j are, respectively, the semiconducting band gap of QDs and energy levels of the exciton, and Γ has been introduced as a phenomenological broadening parameter. The Coulomb interaction energies E_C^j of exciton states Ψ_j are defined by

$$E_C^j = \langle \Psi_j | \frac{e^2}{4\pi\epsilon_0\epsilon_r |\vec{r}_e - \vec{r}_h|} | \Psi_j \rangle. \tag{15}$$

It is helpful for better understanding of the level structures of exciton states in CQDs to use the Coulomb energies E_C^j and the electron and hole tunnelling energies $t_{i=e,h} = \frac{1}{2}(E_i^- - E_i^+)$. Here, E_i^+ and E_i^- are energies of single-carrier bonding and antibonding states, respectively.

We use the von Neumann entropy of entanglement to quantify the degree of entanglement. Then wave functions $\Psi_i(z_e, z_h, \vec{p}_{CM}, \vec{p}_{rel})$ are further expanded in the basis of the direct products of electron and hole orbitals in single dot:

$$\Psi_i = c_1|00\rangle + c_2|01\rangle + c_3|10\rangle + c_4|11\rangle, \tag{16}$$

where the first (second) index of $|ij\rangle$ gives the position of the electron (the hole). $|00\rangle$ and $|11\rangle$ correspond to intradot orbital states where both the electron and hole are in the same QD; $|01\rangle$ and $|10\rangle$ correspond to interdot ones where the electron and the hole are in different QDs. With the use of the expansion coefficients c_i, the reduced density matrix ρ_e (ρ_h) of electron (hole) can be deduced and then the von Neumann entropy[25] of entanglement can be obtained

$$S = -Tr\rho_e \log_2 \rho_e = -Tr\rho_h \log_2 \rho_h. \tag{17}$$

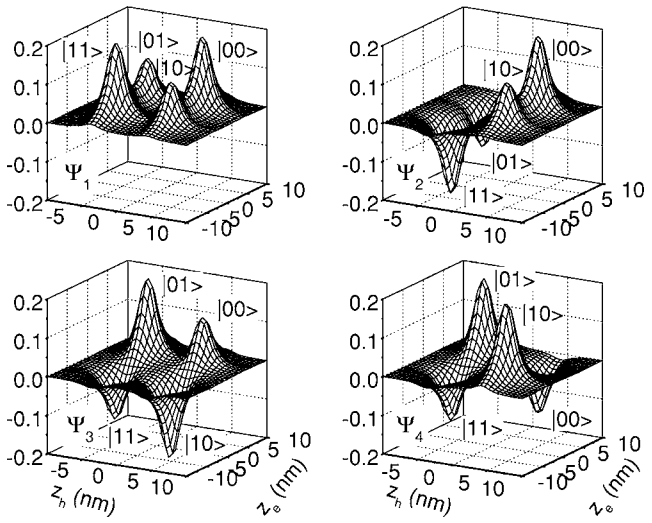

FIG. 2. Wave functions of Ψ_{1-4} in CQDs of $R_0=R_1=10$ nm with $W_b=6$ nm as functions of electron and hole coordinates in z direction.

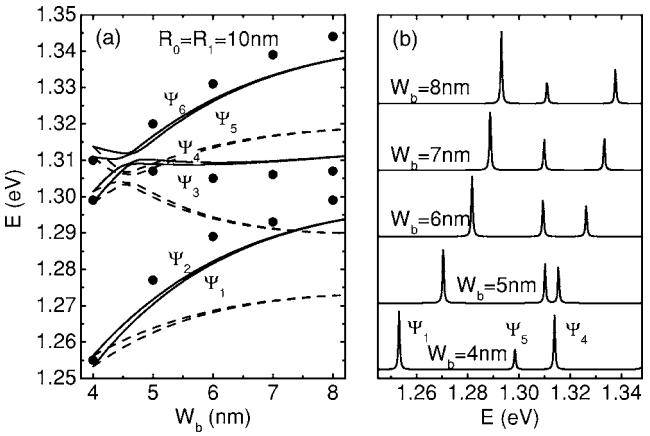

FIG. 3. (a) Energy levels of Ψ_{1-6} for CQDs of $R_0=R_1=10$ nm as functions of barrier width W_b. The solid and dashed lines correspond to the model with a variable W_d as shown in Fig. 1(b) and with a fixed $W_d=2$ nm. The filled circles are experimental data extracted from Ref. 6. (b) Optical spectra for $W_b=4$, 5, 6, 7, and 8 nm, respectively.

III. ENERGY LEVELS AND OPTICAL TRANSITIONS

To compare the calculated results of heavy-hole excitons with the experiments,[6] we take the material parameters of InGaAs/GaAs CQDs as $m_e^*=0.043m_e$, $m_h^*=7m_e^*$, $\varepsilon_r=13.5$, $V_e=0.53$ eV, $V_h=0.175$ eV, and $E_g=0.814$ eV. The size of QDs is chosen to resemble the experimental system where $W_d\approx 2$ nm and $R_{0,1}\approx 10$ nm, as shown in Fig. 1.

Four s-shell exciton states Ψ_{1-4} and two p-shell ones $\Psi_{5,6}$ in coupled identical QDs with $R_0=R_1=10$ nm are calculated. The wave functions of Ψ_{1-4} in the CQDs of $W_b=6$ nm are shown in Fig. 2. It can be seen that the symmetric bonding and antisymmetric antibonding exciton states are formed. $\Psi_{1,2}$ are intradot s exciton states with the main components of $|00\rangle$ and $|11\rangle$, while $\Psi_{3,4}$ are interdot ones with the main components of $|01\rangle$ and $|10\rangle$. $\Psi_{5,6}$ are intradot p exciton states. In Fig. 3(a), energy levels are plotted as functions of barrier width W_b for Ψ_{1-4} and $\Psi_{5,6}$ in the CQDs. Two kinds of energy splittings can be seen between exciton states. The small ones, such as those between Ψ_1 and Ψ_2, are only several meV for small W_b and decrease to zero with increasing W_b. The large ones, such as those between Ψ_1 and Ψ_4, can be several tens meV for small W_b and remain large values even for large W_b. With decreasing W_b, the intradot exciton states $\Psi_{1,2}$ and $\Psi_{5,6}$ show similar red shifts, while the interdot ones $\Psi_{3,4}$ show blueshifts. It is found that the values of the red and blue shifts are very sensitive to the variation of W_d with W_b. As W_b changes from 8 to 4 nm, the calculated blue shift of Ψ_4 (24 meV) is much larger than the experimental one (3 meV)[6] if the fixed $W_d=2$ nm is taken. Both the calculated redshifts (40 meV) and blue ones (3 meV) can be in good agreement with the experimental ones as shown in Fig. 3(a) if the variation of W_d with W_b shown in Fig. 1(b) is considered. In Fig. 3(b), the spectra are plotted for $W_b=4$, 5, 6, 7, and 8 nm, respectively. It can be seen that only the symmetric states Ψ_1, Ψ_4, and Ψ_5 are optically active; the antisymmetric ones are optically inactive. Thus, the splittings between the bright and dark states cannot be seen in the spectra. With increasing W_b, the transition intensity of the intradot exciton state Ψ_1 remains unchanged while that of the interdot exciton state Ψ_4 decreases.

In order to better understand the spectrum structures of CQDs, both the tunneling and Coulomb energies are given as functions of W_b in Fig. 4. The electron tunneling energy t_e is much larger than the hole one t_h since m_e^* is much less than m_h^*. At $W_b=4$ nm, for example, $t_e=27$ meV and $t_h=1.8$ meV. With increasing W_b, both t_e and t_h decrease exponentially. Coulomb energies E_C^1 (E_C^3) and E_C^2 (E_C^4) of the intradot (interdot) exciton states are almost equal. For small W_b, the differences $\Delta E_C^{1,4}$ ($\Delta E_C^{2,3}$) between E_C^1 (E_C^2) and E_C^4 (E_C^3) are much smaller than t_e so that the electron tunneling strongly influences the exciton levels. As W_b increases, E_C^1 and E_C^2 enhance slowly while E_C^3 and E_C^4 decrease rapidly. As $W_b>6.8$ nm, $\Delta E_C^{1,4}$ ($\Delta E_C^{2,3}$) are larger than t_e and the Coulomb interaction exhibits a more important role for the spectrum structures of CQDs. The large splittings between $\Psi_{1,2}$ and $\Psi_{3,4}$ are just the results of the competition between the electron tunneling and the Coulomb interactions. The small

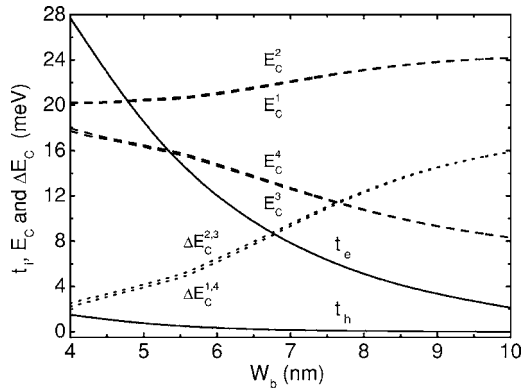

FIG. 4. Electron and hole tunneling energies t_e and t_h (solid lines), Coulomb energies E_C^j (dashed lines), and the differences $\Delta E_C^{i,j}=E_C^i-E_C^j$ (dotted lines) as functions of barrier width W_b.

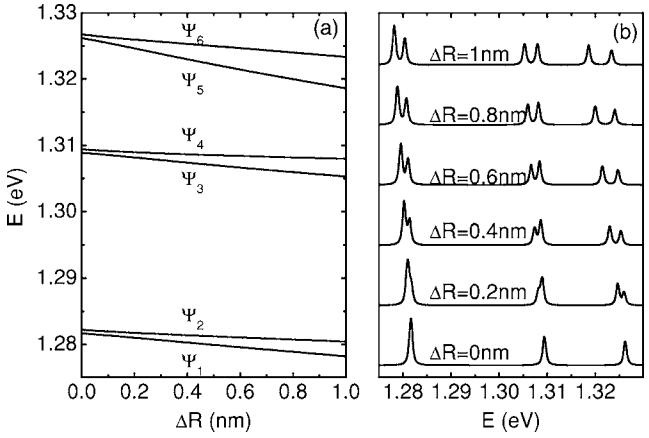

FIG. 5. Variation of energy levels (a) and optical spectra (b) with the dot radius difference ΔR for CQDs of $R_1=10$ nm with $W_b=6$ nm.

splittings, such as those between Ψ_1 and Ψ_2, roughly come from the hole tunneling.

As the symmetry of the CQDs is broken, the energy levels and optical spectra can be greatly changed. For example, we give the variation of exciton levels and spectra with the dot radius difference $\Delta R=R_0-R_1$ in Figs. 5(a) and 5(b). With the increase of ΔR, the splittings, such as those between Ψ_1 and Ψ_2, can be obviously enhanced due to the orbital energy differences. Most importantly, Ψ_{1-6} are all optically allowed because of the mixture of the bright and dark states and additional transition peaks can be seen on the optical spectra as $\Delta R>0.2$ nm. In the PL spectra measured by Bayer *et al.*,[6] such splittings have not been observed, so the radius difference between the two dots should be less than 0.2 nm. The corresponding difference of the band gap between the two dots will be less than 2 meV if the broken symmetry only induced by the composition fluctuation or the strain modification is considered.[18,19]

For exciton states in CQDs, the electric field can be used to tune the energy levels and optical transitions. In Fig. 6(a), energy levels of Ψ_{1-4} in the CQDs of $R_0=R_1=10$ nm with $W_b=8$ nm are plotted as functions of electric field F. The

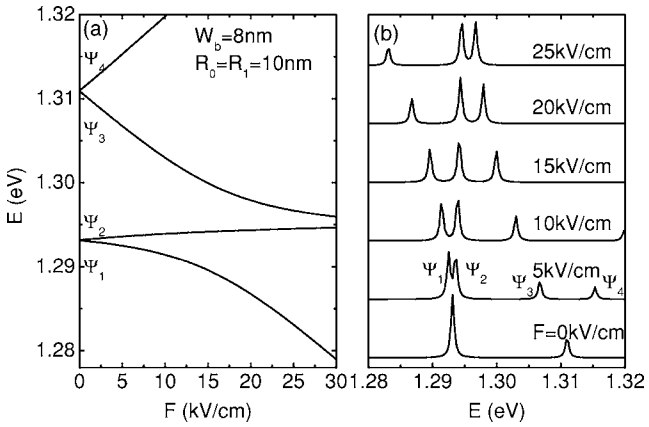

FIG. 6. (a) Energy levels of Ψ_{1-4} in CQDs of $R_0=R_1=10$ nm with $W_b=8$ nm as functions of electric field F. (b) Corresponding optical spectra.

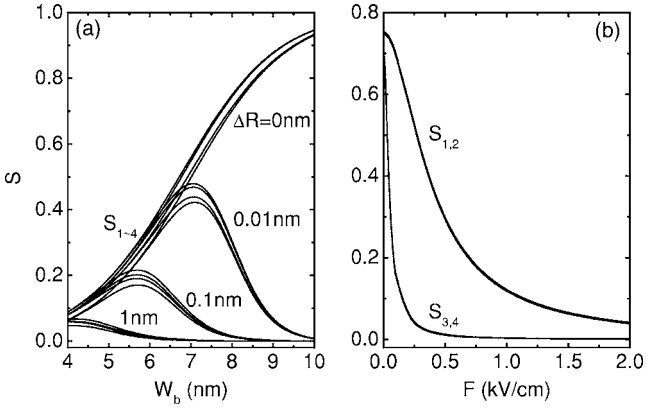

FIG. 7. (a) Entanglement entropies S_{1-4} of Ψ_{1-4} in CQDs of $R_1=10$ nm with $\Delta R=0$, 0.01, 0.1, and 1 nm as functions of barrier width W_b. (b) Those in CQDs of $R_0=R_1=10$ nm with $W_d=8$ nm as functions of electric field F.

interdot exciton states $\Psi_{3,4}$ exhibit strong Stark effects due to their large dipole moments, while the intradot exciton states $\Psi_{1,2}$ exhibit weak ones due to their small dipole moments. A coupling between Ψ_1 and Ψ_3 is induced and enhanced by increasing F, and the energy of Ψ_2 shows a slight increase. At $F=15$ kV/cm, an anticrossing of 10.34 meV occurs between Ψ_1 and Ψ_3. The variation of the optical spectra with F is given in Fig. 6(b). Four s-shell states are all optically allowed due to the broken symmetry induced by the electric field. As shown in Fig. 6(b), Ψ_2 splits from Ψ_1 and exhibits a large transition intensity as $F>5$ kV/cm. With increasing F, the intensity of Ψ_1 decreases and that of Ψ_3 increases, and it can be understood by noting the variation of the coupling and the anticrossing at $F=15$ kV/cm between them. As a matter of fact, the splitting betweenΨ_1 and Ψ_2 and the anticrossing between Ψ_1 and Ψ_3 under an external electric field have been respectively observed by Ortner *et al.*[15] and Krenner *et al.*[16]

IV. ENTANGLEMENT OF EXCITON STATES

A. Entanglement entropy

Entangled exciton states are important for the realization of quantum computation using CQDs. In the basis of single-carrier orbital products, the maximally entangled exciton states, i.e., the Bell states can be written as $\sqrt{2}/2(|00\rangle\pm|11\rangle)$ and $\sqrt{2}/2(|01\rangle\pm|10\rangle)$. Those states, such as $|00\rangle$, $\sqrt{2}/2(|0\rangle\pm|1\rangle)|1\rangle$, $1/2(|0\rangle\pm|1\rangle)(|0\rangle\pm|1\rangle)$, and so on, are completely unentangled ones. Any deviation from the Bell states corresponds to a decrease of entanglement. The degree of entanglement can be quantified by the von Neumann entropy of Eq. (17). The entangle entropy of a maximally entangled exciton state is 1, and that of a completely unentangled state is 0. Based on the calculation of the entanglement entropy, the effects of the symmetry, size, and electric field on the entanglement of exciton states in CQDs can be well investigated.

In Fig. 7(a), the entanglement entropies S_{1-4} are plotted as functions of W_b for four s-shell exciton states Ψ_{1-4} in CQDs

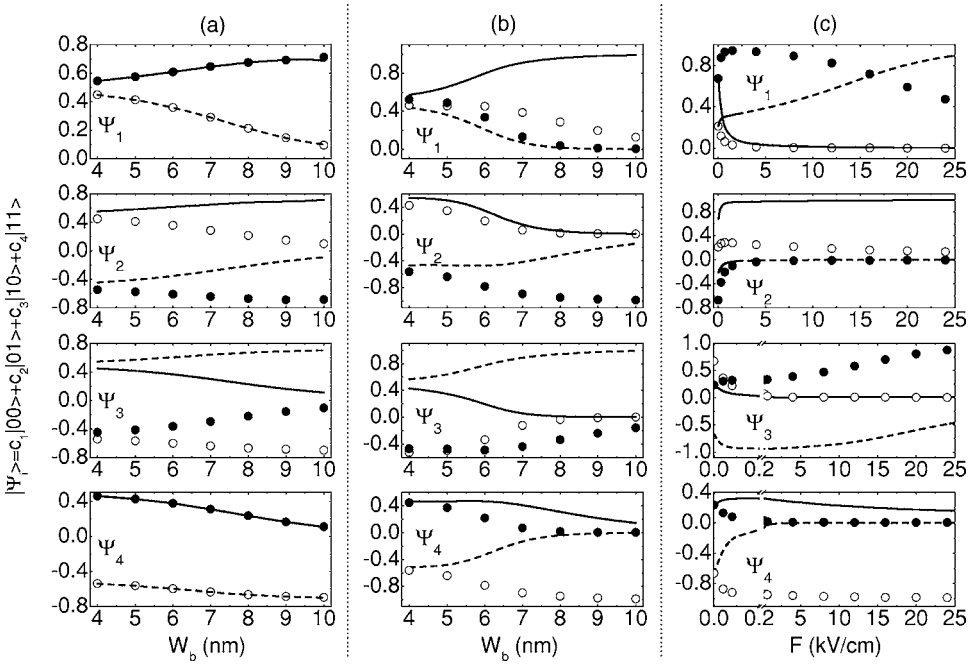

FIG. 8. Expansion coefficients c_{1-4} of Ψ_{1-4} in the basis of orbital products as shown in Eq. (16) for CQDs of $R_1=10$ nm with $R_0=10$ (a) and $R_0=10.1$ (b) as functions of barrier width W_b, and for that of $R_0=R_1=10$ nm with $W_b=8$ nm (c) as functions of electric field F. The coefficients c_1, c_2, c_3, and c_4 are represented by the solid lines, dash lines, circles, and filled circles, respectively. For Ψ_3 and Ψ_4 in (c), breaks at $F=0.2$ kV/cm have been taken to clearly show the variation of the coefficients in the region of small F.

of $R_1=10$ nm with $\Delta R=0$, 0.01, 0.1, and 1 nm, respectively. There are few differences between the entropies S_{1-4}. As W_b is small, the S_{1-4} are small for both coupled identical and nonidentical CQDs. For coupled identical QDs, the S_{1-4} increase monotonously with increasing W_b and exceed 0.9 as $W_b>10$ nm. However, the large entanglement for coupled identical QDs of large W_b is very fragile and easily destroyed by the broken symmetry. For coupled nonidentical QDs of $\Delta R=0.01$ nm, the S_{1-4} achieve their maximum of about 0.4 at $W_b=7$ nm, and decrease rapidly with further increasing W_b. The S_{1-4} can be greatly reduced by increasing ΔR.

The entanglements of exciton states in CQDs can be strongly destroyed by the broken symmetry induced by an electric field F, as shown in Fig. 7(b). The F of 1.5 kV/cm makes $S_{1,2}$ decrease to 0.1 while the F of 0.2 kV/cm makes $S_{3,4}$ decrease to 0.1. It is because of quite different Stark effects of the intra- and interdot exciton states. The exciton states are almost unentangled at the $F=F_{anti}$ where the anticrossing between Ψ_1 and Ψ_3 appears.

Here, only the entanglements of the heavy-hole exciton states are involved. For light-hole exciton states, the entanglement of both bonding and antibonding states can be notably changed by the enhancement of the hole tunneling. Therefore, the entanglements of low-lying exciton states may be somewhat influenced by the heavy- and light-hole mixing which strongly depends on the size and barrier width of the CQDs. However, the hole ground state of CQDs resembling the experimental system of Bayer *et al.*[6] is dominantly heavy-hole-like.[19] The influence of the heavy- and light-hole mixing in our studies is small. Nevertheless, the mixing needs to be considered for CQDs with larger size and smaller barrier width.

B. Evolution of orbital occupations

The behavior of entanglements in CQDs mentioned above can be well understood from the variation of the orbital occupations of the exciton states. In Fig. 8(a), the expansion coefficients of Ψ_{1-4} in Eq. (16) are plotted as functions of W_b for the coupled identical QDs. It can be clearly seen that the same kinds of orbital states contribute the same strength to an exciton state due to their identical orbital energies. As W_b is small, the intradot orbital states $|00\rangle$ and $|11\rangle$ and the interdot ones $|01\rangle$ and $|10\rangle$ are all mixed into an exciton state. It leads to a large deviation from the Bell exciton states so that small entanglements are shown. It is interesting to note that the coupling of the intra- and interdot orbital states, for example, that of $|00\rangle$ and $|10\rangle$, depends strongly on both the electron tunneling energy t_e and the difference of Coulomb interaction energies between them. With increasing W_b, such couplings decrease because of the decrease of t_e and the increase of $\Delta E_C^{i,j}$ as shown in Fig. 4. As $W_b>7$ nm ($\Delta E_C^{i,j}>t_e$), the main component of Ψ_i is larger than 83 % and the four s states are close to the exciton Bell states. However, such large entanglements for large W_b are very fragile because of $m_h^* \gg m_e^*$. This can be well understood if we notice that the exciton tunelings between $|00\rangle$ and $|11\rangle$ or between $|01\rangle$ and $|10\rangle$ are mainly determined by the hole (the heavy carrier) tunneling, which is very weak, as shown in Fig. 4. This makes the couplings of the same kinds of orbital states easily destroyed by even a small orbital energy difference. Such an effect is clearly shown in Fig. 8(b) for coupled nonidentical QDs of $R_0=10.1$ nm and $R_1=10$ nm. For short W_b, the four orbital states are mixed into an exciton state with various probabilities. With increasing W_b, the couplings be-

tween $|00\rangle$ and $|11\rangle$ or between $|01\rangle$ and $|10\rangle$ decrease rapidly, and the hole comes to be localized in one of the two QDs. As $W_b > 7$ nm, Ψ_{1-4} are respectively close to the four simple orbital products which are unentangled.

The variation of orbital occupations of exciton states with electric field F is given in Fig. 8(c). With increasing F, the large entangled exciton states Ψ_{1-4} quickly approach the simple orbital products. At $F=1.5$ kV/cm, Ψ_1 (Ψ_2) is close to $|11\rangle$ ($|00\rangle$), and at $F=0.2$ kV/cm, Ψ_3 (Ψ_4) is close to $|01\rangle$ ($|10\rangle$). As F increases further, a coupling between $|11\rangle$ and $|01\rangle$ appears in both Ψ_1 and Ψ_3. At $F=15$ kV/cm, Ψ_1 and Ψ_3, respectively, approach $\sqrt{2}/2(|11\rangle+|01\rangle)$ and $\sqrt{2}/2(|11\rangle-|01\rangle)$, which corresponds to an anticrossing in the spectra as shown in Fig. 6. It is clear that such a coupling only arises from the electron tunneling while the hole remains localized in the QD1. Then Ψ_1 and Ψ_3 are almost unentangled.

V. SUMMARY AND CONCLUSION

To efficiently calculate the exciton states in vertically coupled InGaAs/GaAs QDs, a VD method is proposed. In the method, a set of variational basis is formed by solving a trial zeroth-order Hamiltonian which includes the variational confining potential and effective Coulomb term. The appropriate basis, the eigensolutions of the total Hamiltonian and the minimal ground state energy are simultaneously determined by both the variation method and the exact diagonalization with use of the basis. Based on the method, the measured optical spectra can be well reproduced with the use of reasonable band and structural parameters.

By considering the variation of dot height with barrier width for coupled identical QDs, the exciton energy splittings and shifts of the calculated spectra with decreasing barrier width are in good agreement with the measurements.[6] For coupled identical QDs, the energy splittings are caused by the carrier tunneling and the difference of Coulomb interaction energies between the intra- and interdot exciton states, and only the bonding states are optically active. As the symmetry is broken, the splittings are enhanced and all four *s*-shell states are optically allowed. The coupling of exciton states is strongly influenced by an electric field. A resonant tunneling between electron orbitals can appear at a specific electric field, which corresponds to an anticrossing in the spectra.

The entanglements of exciton states in CQDs are investigated by calculating the entanglement entropies and analyzing the orbital occupations. At small barrier widths, large couplings between the intra- and interdot orbital states exist in exciton states so that entanglements are small. For coupled identical QDs, large entanglements can appear at large barrier widths. However, such large entanglements are very fragile because the couplings between the intradot orbitals or between the interdot ones strongly depend on the hole (the heavy carrier) tunneling, which is very weak. As the symmetry is broken by the dot differences, a slight orbital energy difference can reduce the couplings between the same kinds of orbitals to cause the decrease of the entanglements. Therefore, it is difficult to obtain large exciton entanglements in coupled nonidentical QDs without controlled external fields if the hole is much heavier than the electron.

Finally, we should point out that the effects of structural and electronic parameters within a realistic multiband model and those of external fields on the entanglement of the qubits are worthwhile to investigate. How to realize stably and controllably entangled qubits is one of the most important research subjects in the development of solid-state quantum computers.

ACKNOWLEDGMENT

Financial support from NSF China (Grant No. 10374057) and China's "863" Programme is gratefully acknowledged.

*Electronic address: zjl-dmp@tsinghua.edu.cn

[1] D. Loss and D. P. DiVincenzo, Phys. Rev. A **57**, 120 (1998).
[2] A. Imamoglu, D. D. Awschalom, G. Burkard, D. P. DiVincenzo, D. Loss, M. Sherwin, and A. Small, Phys. Rev. Lett. **83**, 4204 (1999).
[3] D. P. DiVincenzo, D. Bacon, J. Kempe, G. Burkard, and K. B. Whaley, Nature (London) **408**, 339 (2000).
[4] D. Loss and E. V. Sukhorukov, Phys. Rev. Lett. **84**, 1035 (2000).
[5] P. Hawrylak, S. Fafard, and Z. R. Wasilewski, Condens. Matter News **7**, 16 (1999).
[6] M. Bayer, P. Hawrylak, K. Hinzer, S. Fafard, M. Korkusinski, Z. R. Wasilewski, O. Stern, and A. Forchel, Science **291**, 451 (2001).
[7] J. I. Cirac and P. Zoller, Phys. Rev. Lett. **74**, 4091 (1995); C. Monroe, D. M. Meekhof, B. E. King, W. M. Itano, and D. J. Wineland, *ibid.* **75**, 4714 (1995).
[8] N. A. Gershenfeld and I. L. Chuang, Science **275**, 350 (1997); D. G. Cory, A. F. Fahmy, and T. F. Havel, Proc. Natl. Acad. Sci. U.S.A. **94**, 1634 (1997); E. Knill, I. Chuang, and R. Laflamme, Phys. Rev. A **57**, 3348 (1998); I. L. Chuang, N. Gershenfeld, and M. Kubinec, Phys. Rev. Lett. **80**, 3408 (1998); J. A. Jones, M. Mosca, and R. H. Hansen, Nature (London) **393**, 344 (1998).
[9] Q. A. Turchette, C. J. Hood, W. Lange, H. Mabuchi, and H. J. Kimble, Phys. Rev. Lett. **75**, 4710 (1995).
[10] D. V. Averin, Solid State Commun. **105**, 659 (1998); A. Shnirman, G. Schön, and Z. Hermon, Phys. Rev. Lett. **79**, 2371 (1997).
[11] G. D. Sanders, K. W. Kim, and W. C. Holton, Phys. Rev. A **60**, 4146 (1999).
[12] P. Borri, W. Langbein, U. Woggon, M. Schwab, M. Bayer, S. Fafard, Z. Wasilewski, and P. Hawrylak, Phys. Rev. Lett. **91**, 267401 (2003).
[13] Z. R. Wasilewski, S. Fafard, and J. P. McCaffrey, J. Cryst. Growth **201**, 1131 (1999).
[14] G. Ortner, M. Schwab, P. Borri, W. Langbein, U. Woggon, M. Bayer, S. Fafard, Z. Wasilewski, P. Hawrylak, Y. B. Lyanda-Geller, T. L. Reinecke, and A. Forchel, Physica E (Amsterdam) **25**, 256 (2004).

[15] G. Ortner, M. Bayer, Y. Lyanda-Geller, T. L. Reinecke, A. Kress, J. P. Reithmaier, and A. Forchel, Phys. Rev. Lett. **94**, 157401 (2005).
[16] H. J. Krenner, M. Sabathil, E. C. Clark, A. Kress, D. Schuh, M. Bichler, G. Abstreiter, and J. J. Finley, Phys. Rev. Lett. **94**, 057402 (2005).
[17] M. Korkusinski, P. Hawrylak, M. Bayer, G. Ortner, A. Forchel, S. Fafard, and Z. Wasilewski, Physica E (Amsterdam) **13**, 610 (2002).
[18] G. Bester, J. Shumway, and A. Zunger, Phys. Rev. Lett. **93**, 047401 (2004).
[19] G. Bester, A. Zunger, and J. Shumway, Phys. Rev. B **71**, 075325 (2005).
[20] J.-L. Zhu, J. J. Xiong, and B.-L. Gu, Phys. Rev. B **41**, 6001 (1990).
[21] J.-L. Zhu, Z. Q. Li, J. Z. Yu, K. Ohno, and Y. Kawazoe, Phys. Rev. B **55**, 15819 (1997).
[22] W. Que, Phys. Rev. B **45**, 11036 (1992).
[23] J. Song and S. E. Ulloa, Phys. Rev. B **52**, 9015 (1995).
[24] G. W. Bryant, Phys. Rev. B **37**, 8763 (1988).
[25] C. H. Bennett, H. J. Bernstein, S. Popescu, and B. Schumacher, Phys. Rev. A **53**, 2046 (1996).